Eur. Phys. J. C 25, 391–403 (2002)
Digital Object Identifier (DOI) 10.1007/s10052-002-1032-9

THE EUROPEAN PHYSICAL JOURNAL C

Ways to detect a light Higgs boson at the LHC

A. De Roeck[1], V.A. Khoze[2,3], A.D. Martin[2], R. Orava[4], M.G. Ryskin[2,3]

[1] CERN, 1211 Geneva 23, Switzerland
[2] Institute for Particle Physics Phenomenology, University of Durham, Durham DH1 3LE, UK
[3] Petersburg Nuclear Physics Institute, Gatchina, St. Petersburg, 188300, Russia
[4] Department of Physical Sciences, University of Helsinki, and Helsinki Institute of Physics, Finland

Received: 5 July 2002 /
Published online: 30 August 2002 –

Abstract. We summarize the possible processes which may be used to search for a Higgs boson, of mass in the range 114–130 GeV, at the LHC. We discuss, in detail, two processes with rapidity gaps: exclusive Higgs production with tagged outgoing protons and production by Weak Boson Fusion, in each case taking $H \to b\bar{b}$ as the signal. We make an extensive study of all possible $b\bar{b}$ backgrounds, and discuss the relevant experimental issues. We emphasize the special features of these signals, and of their background processes, and show that they could play an important role in identifying a light Higgs boson at the LHC.

1 Introduction

The identification of the Higgs boson(s) is one of the main goals of the Large Hadron Collider (LHC) being constructed at CERN. According to current theoretical prejudice it is likely that a Higgs boson will exist in the mass range $114 < M_H < 135$ GeV. In the Standard Model description of electroweak data, the virtual effects favour a Higgs with mass at, or just above, the LEP bound of 114 GeV. Moreover, in the Minimal Supersymmetric Model a scalar Standard-Model-like Higgs boson with mass below 135 GeV should exist[1]. However, the experimental detection of such a 'light' Higgs boson at the LHC will be challenging. There is no obvious perfect detection process. Rather there is a range of complementary possibilities, as illustrated in Table 1. The Table shows the number of identified Higgs events and the number of background events, for a Standard Model Higgs boson of mass $M_H = 120$ GeV for the integrated luminosity of 30 fb^{-1} planned for the first two or three years of LHC running, for each of the various proposed detection channels. A glance at the Table shows that, *either* large signals are accompanied by a huge background, *or* the processes have comparable signal and background rates for which the number of Higgs events is rather small.

Besides containing the conventional processes for the detection of a light Higgs boson, the Table also lists processes (c,d,f) with a rapidity gap on either side of the boson, which provide a clean environment for its production. These processes are often overlooked, but they have special advantages. Here we shall study two of these processes in detail.

First, in Sect. 2, we discuss the exclusive process $pp \to p + H + p$, where the + sign indicates the presence of a rapidity gap. We show that it is possible to tag the outgoing protons such that the Higgs may be identified, and its mass measured to an accuracy of about 1 GeV, using the 'missing mass' method. That is using tagged protons we have $M_H = M_{\rm missing}$ with $\Delta M_{\rm missing} \sim 1\,{\rm GeV}$. Importantly, the process allows an independent measurement of the Higgs mass via the $H \to b\bar{b}$ decay, $M_H = M_{b\bar{b}}$, although now the resolution is much poorer with $\Delta M_{b\bar{b}} \sim 10$GeV. The existence of matching peaks, centred about $M_{\rm missing} = M_{b\bar{b}}$, is a unique feature of the exclusive diffractive Higgs signal[2]. Besides its obvious value in identifying the Higgs and in sharpening the determination of its mass, we will see that the mass equality also plays a key role in reducing background contributions. Another advantage of the $H \to b\bar{b}$ signal is that, at leading order, the $gg \to b\bar{b}$ background process is suppressed by a $J_z = 0$ selection rule, see Sect. 2.3 [8,9].

Of course, we have to pay a price for the survival of the rapidity gaps, so the event rate is low. Nevertheless the process has the advantage that the signal exceeds the background. The absolute value of the $pp \to p + H + p$ cross section has been calculated in [4,10]. The derivation is outlined in Sect. 2.1. Moreover the predicted value can be checked experimentally by measuring the rate of the double-diffractive production of dijets (of comparable mass). The uncertainties of the calculation of the $pp \to p + H + p$ cross section are discussed in Sect. 2.2.

[1] A discussion of, and references for, the current status of allowed masses and other properties of Higgs bosons can be found, for example, in [1]

[2] This may be contrasted with the search for a Higgs peak sitting on a huge background in the $M_{\gamma\gamma}$ spectrum, see process (a) of Table 1

Table 1. The number of signal and background events for various methods of Higgs detection at the LHC. The significance of the signal is also given. The mass of the Higgs boson is taken to be 120 GeV and the integrated luminosity is taken to be 30 fb^{-1}. The notation gg^{PP} is to indicate that the gluons originate within overall colour-singlet (hard Pomeron) t-channel exchanges; see, for example, Fig. 1. The entries for the various processes are taken, or scaled from the results for 100 fb^{-1} luminosity, from references (a) [2], (b) [3], (d) [4], (e) [2,5], (g,h) [2] and (i) [6], where the K factors have been omitted. Processes (c) and (f) are discussed in detail in Sects. 2 and 3, respectively, of this paper. A detailed study of the NLO contributions to the irreducible background to the $H \to \gamma\gamma$ signal shows the K factor is 0.65 that of the signal [7]. Taking these K factors into account the authors find that the significance of the $H \to \gamma\gamma$ signal may increase to 7σ

Higgs signal		number of events signal	background	S/B	significance $S/\sqrt{S+B}$
a) $H \to \gamma\gamma$	CMS	313	5007	$0.06\left(\frac{1\,\text{GeV}}{\Delta M_{\gamma\gamma}}\right)$	4.3σ
	ATLAS	385	11820	$0.03\left(\frac{2\,\text{GeV}}{\Delta M_{\gamma\gamma}}\right)$	3.5σ
b) $t\bar{t}H$ $\hookrightarrow b\bar{b}$		26	31	$0.8\left(\frac{10\,\text{GeV}}{\Delta M_{b\bar{b}}}\right)$	3σ
c) $gg^{PP} \to p + H + p$ $\hookrightarrow b\bar{b}$		11	4	$3\left(\frac{1\,\text{GeV}}{\Delta M_{\text{missing}}}\right)$	3σ
d) $gg^{PP} \to X + H + Y$ $\hookrightarrow b\bar{b}$		190	21,000	$0.009\left(\frac{10\,\text{GeV}}{\Delta M_{b\bar{b}}}\right)$	1.3σ
e) Weak Boson Fusion (WBF)					
$qWWq \to jHj \to j\gamma\gamma j$		17	9	CMS	3.3σ
		18	17	ATLAS	3σ
	$\to j\tau\tau j$	25	8		4.4σ
	$\to jW(l\nu)W^*(l\nu)j$	49	31		5.4σ
f) WBF with rapidity gaps		jet E_T cuts:			
$qWWq \to j + H(\text{high}\, q_t) + j$ $\hookrightarrow b\bar{b}$		250	1800	$0.14\left(\frac{10\,\text{GeV}}{\Delta M_{b\bar{b}}}\right)$	5.5σ
		Higgs q_t cut:			
		400	3700	$0.11\left(\frac{10\,\text{GeV}}{\Delta M_{b\bar{b}}}\right)$	6.2σ
g) $gg \to ZZ^* \to 4l$		6	4	CMS	1.9σ
		3	1.5	ATLAS	1.4σ
h) $gg \to WW^* \to l\nu l\bar{\nu}$		44	272	CMS	2.5σ
i) $WH \to l\nu b\bar{b}$		161	7095	0.02	1.9σ

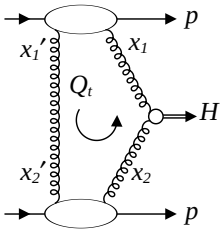

Fig. 1. Schematic diagram of the exclusive double-diffractive production of a Higgs boson, that is the process $pp \to p+H+p$, in which the + signs indicate the presence of rapidity gaps

Equally important to the calculation of the exclusive double-diffractive $p + (H \to b\bar{b}) + p$ signal, is the estimation of the $b\bar{b}$ background. The background processes are found to be suppressed by their spin and colour structure, and are interesting in their own right. The various sources of the background are discussed in Sects. 2.3 and 2.4. First, in Sect. 2.3, we summarize the sources, together with their sizes relative to the Higgs signal, and then, in Sect. 2.4, we give the detailed justification of the results. Section 2.5 is devoted to a study of production by soft Pomeron-Pomeron collisions. We find that it gives a negligible contribution both to the exclusive $H \to b\bar{b}$ signal and to the background. In Sect. 2.6, we turn to a discussion of the experimental issues connected with the exclusive diffractive signal. We study the experimental efficiencies, the choice of cuts, the accurate determination of the 'missing mass' via the measurement of the forward protons and, finally, the problems connected with the 'pile-up' of multiple interactions in each beam crossing.

The second process that we study is the central production of a Higgs boson via WW fusion

$$pp \to qWWq \to \text{jet} + H + \text{jet},$$

see Sect. 3. We may suppress the background to this process by exploiting the fact that the cross section is rather flat as a function of the transverse momentum, q_t, of the Higgs boson, on account of the large W boson mass. Moreover, since this process is mediated by t channel W exchange, which is a point-like colourless object, there is no corresponding bremsstrahlung in the central region [11–14] and hence no Sudakov suppression of the rapidity gaps.

2 Exclusive diffractive $H \to b\bar{b}$ production

In this section we make a detailed study of the third process of Table 1, namely [10,9]

$$pp \to p + H + p$$

where the Higgs decays via the $b\bar{b}$ mode. We assume that the outgoing protons and the b and $\bar{b}$ jets can be identified and measured, and that there are no other particles in the final state. We quantify both the signal and the background for this exclusive process and, moreover, discuss the relevant experimental issues.

2.1 Calculation of the $p + H + p$ cross section

The basic mechanism for the process is shown in Fig. 1. It turns out that the typical values of the transverse momentum Q_t of the gluon, which screens the colour, are much smaller than M_H, but are yet sufficiently large for perturbative QCD to be applicable. The amplitude is [10, 9]

$$\mathcal{M} = A\pi^3 \int \frac{d^2Q_t}{Q_t^4} f_g\left(x_1, x_1', Q_t^2, \frac{M_H^2}{4}\right) \times f_g\left(x_2, x_2', Q_t^2, \frac{M_H^2}{4}\right) \quad (1)$$

where the f_g's are the skewed unintegrated gluon densities of the proton, and where the $gg \to H$ vertex factor is

$$A^2 = K\frac{\sqrt{2}G_F}{9\pi^2}\alpha_S^2(M_H^2) \quad (2)$$

with the NLO K factor $K \simeq 1.5$. The longitudinal momentum fractions carried by the gluons satisfy

$$\left(x' \sim \frac{Q_t}{\sqrt{s}}\right) \ll \left(x \sim \frac{M_H}{\sqrt{s}}\right) \ll 1 \quad (3)$$

where, for the LHC, $\sqrt{s} = 14$ TeV. In this domain the skewed unintegrated densities are given in terms of the conventional (integrated) densities $g(x, Q_t^2)$. To single log accuracy, we have [10]

$$f_g\left(x, x', Q_t^2, \frac{M_H^2}{4}\right) = R_g \frac{\partial}{\partial \ln Q_t^2}\left(\sqrt{T\left(Q_t, \frac{M_H}{2}\right)} x g\left(x, Q_t^2\right)\right) \quad (4)$$

where $T(Q_t, \mu)$ is the survival probability that the gluon remains untouched in the evolution up to the hard scale $\mu = M_H/2$. This Sudakov factor T is the result of resumming the virtual contributions in the DGLAP evolution. It is given by

$$T(Q_t, \mu) = \exp\left(-\int_{Q_t^2}^{\mu^2} \frac{\alpha_S(k_t^2)}{2\pi}\frac{dk_t^2}{k_t^2}\int_0^{\mu/(\mu+k_t)} \times \left[zP_{gg}(z) + \sum_q P_{qg}(z)\right] dz\right). \quad (5)$$

The square root of T arises in (4) because the survival probability is only relevant to the hard gluon. Note that the gluon with $x' \simeq 0$ is almost 'at rest' and so there is no possibility of QCD radiation [15]. The multiplicative factor R_g is the ratio of the skewed $x' \ll x$ integrated distribution to the conventional diagonal density. For $x \ll 1$ the factor is completely determined [16]. We find $R_g \simeq 1.2$ at the energy of the LHC.

The radiation associated with the $gg \to H$ hard subprocess is not the only means to populate and to destroy the rapidity gaps. There is also the possibility of

soft rescattering in which particles from the underlying event populate the gaps. The probability, S^2, that the gaps survive the soft pp rescattering was calculated using a two-channel eikonal model, which incorporates high mass diffraction [17]. The parameters of the model were obtained from a global analysis of all available soft pp (and $p\bar{p}$) scattering data. In this way, we find $S^2 = 0.02$ for the process $p + H + p$ at the LHC. Including this factor, the cross section is predicted to be [4]

$$\sigma(pp \to p + H + p) \simeq 3 \text{ fb} \tag{6}$$

for the production of a Standard Model Higgs of mass 120 GeV at the LHC.

In Sect. 2.2 we estimate a factor of two uncertainty in the cross section prediction given in (6). On the other hand it is frequently quoted that the predictions of the cross section for diffractive Higgs production cover many orders of magnitude, and for this reason the many authors choose not to consider this Higgs signal. This is unfortunate. Sometimes the rates of different diffractive mechanisms are compared. Sometimes models are used to predict the exclusive signal which are not valid. Indeed, care must be taken when comparing the theoretical predictions for the exclusive $pp \to p + H + p$ process with the results of Monte Carlo simulations. For example, when implementing the Soft Colour Interaction (SCI) prescription [18] in PYTHIA [19], it was found [20] that hard production in single diffractive processes observed at the Tevatron could be described reasonably well, but that the generator hardly ever produces any 'double-Pomeron-exchange' events. Finally, an extremely low limit was claimed [21] for the exclusive $pp \to p + H + p$ cross section.

The fact that such a generator yields an extremely low probability for exclusive processes is not surprising. The generator was created to simulate *inelastic* processes. It operates by starting from the hard subprocess and generates the parton showers by backward evolution. The generator never accounts for the important coherence between different parton showers, nor for the colourless nature of the initial particles. The incoming protons are just considered as a system of coloured partons. As a consequence, the probability not to emit additional secondary jets (and so to reproduce an exclusive process) turns out to be negligibly small. In particular, such a generator is unable to reproduce the elastic cross section. Such generators create many secondary minijets at the parton shower stage and the probability to screen all these minijets by colour interchange is extremely low. Such generators were not constructed to reproduce exclusive processes, where the colour coherence effects and colourless nature of the incoming hadrons are important.

2.2 Uncertainty in the cross section prediction

Note that, in principle, (6) is an absolute prediction for $\sigma(p + H + p)$. Of course, the various inputs are subject to uncertainty. Let us discuss these in turn. First we have the large suppression from the probability $S^2 = 0.02$ that the rapidity gaps survive soft pp rescattering. From the analysis [17] of all soft pp data we estimate the accuracy of the prediction for S^2 is $\pm 50\%$. One check of the eikonal model calculations of S^2 is the estimate of the diffractive dijet production rate measured by the CDF collaboration [22] at the Tevatron. The rate, when calculated using factorization and the diffractive structure functions obtained from HERA data, lies about a factor of 10 above the CDF data. However, when rescattering corrections are included, and the survival probabilities computed, remarkably good agreement with the CDF measurements is obtained [23]. There is, perhaps, a small tendency that an even stronger suppression is required, so the true survival probabilities S^2 may be a bit smaller than our predictions.

Second, although, on account of the Sudakov form factor, the Q_t integral in (1) is infrared safe, the cross section may have some contribution from the non-perturbative region. Again, we expect an accuracy of $\pm 50\%$, but in this case the + sign looks more realistic. The uncertainties in the gluon densities f_g in the integrand are estimated at $\pm 5\%$, leading to a $\pm 22\%$ error on the cross section. This estimate takes into account the accuracy of the value of R_g and the uncertainty on the integrated gluon density xg, at $x \sim 0.01$ relevant to the LHC. Finally, we have NLO contributions to the Sudakov T factor ($\pm 20\%$) and NNLO corrections to the $gg \to H$ vertex factor ($\pm 20\%$). Adding these errors in quadrature gives a *factor two* uncertainty in (6).

We stress that the predicted value of the cross section can be checked experimentally. All the ingredients, except for the NLO correction to the $gg \to H$ vertex, are the same for our signal as for exclusive double-diffractive dijet production, $pp \to p + \text{dijet} + p$, where the dijet system is chosen in the same kinematic domain as the Higgs boson, that is $M(jj) \sim 120$ GeV [4,10]. Therefore by observing the larger dijet production rate, we can confirm, or correct, the estimate of the exclusive Higgs signal.

Of course, so far our discussion has been within the confines of the Standard Model. We should not overlook the possibility that the exclusive Higgs signal may reveal New Physics. For example, the Higgs cross section will be 4 (or even 9) times larger if there were to exist a fourth doublet containing one (or two) quarks heavier than the Higgs.

2.3 Summary of the backgrounds to the $p + (H \to b\bar{b}) + p$ signal

For a light Higgs boson the dominant decay channel is $H \to b\bar{b}$. However, it is impossible to observe this decay in an inclusive process at the LHC, since it is overwhelmed by a huge QCD $b\bar{b}$ background. The advantage of exclusive double-diffractive Higgs production with forward going protons is that there exists a $J_z = 0$, parity even, selection rule, which strongly suppresses the leading order $gg^{PP} \to b\bar{b}$ background subprocess. The PP superscript is to indicate that each gluon comes from a colour-singlet t channel state. One way to see the $J_z = 0$ selection rule is to note that, in the equivalent gluon approach (or in

a planar gauge), the polarisation vectors of the t channel gluons in Fig. 1 are aligned along the transverse component of the loop momentum $\vec{Q}_t$ [4,9]. Integrating over $\vec{Q}_t$ leads to the amplitude $\mathcal{M}$ of the gg^{PP} fusion subprocess being formed from the average over the two transverse polarisations $\varepsilon_1, \varepsilon_2$ of the incoming gluons

$$\mathcal{M} = \frac{1}{2} \sum_{\varepsilon_1,\varepsilon_2} \mathcal{M}(\varepsilon_1, \varepsilon_2)\delta_{\varepsilon_1,\varepsilon_2}. \tag{7}$$

The delta symbol reflects the $J_z = 0$, parity even, character of the di-gluon gg^{PP} incoming state. For *colour-singlet* $b\bar{b}$ production the Born-level contributions of Figs. 2a and b cancel each other, in the massless $m_b \to 0$ limit, due to summation (7). More generally, as a consequence of helicity conservation, and P and T invariance, for the real parts of the $J_z = 0$ $gg^{PP} \to b\bar{b}$ amplitudes [24], the corresponding contributions to the cross section vanish with decreasing quark mass as m_b^2/E_T^2, where $E_T \sim M_H/2$ is the transverse energy of the b or $\bar{b}$ jet.

It is convenient, first, to list the possible sources of the $b\bar{b}$ background to the exclusive $p + (H \to b\bar{b}) + p$ Higgs signal and to state the size of each background in terms of the signal. The justification for the numerical values is given in the next Sect. 2.4. We quote the B/S using the anticipated missing mass resolution, $\Delta M_{\text{missing}} = 1\,\text{GeV}$, expected from employing taggers for the outgoing protons.

At leading order (LO) there are $gg^{PP} \to$"$b\bar{b}$" background contributions, despite the $J_z = 0$ selection rule, which we summarize below.

(i) The prolific $gg^{PP} \to gg$ subprocess may mimic $b\bar{b}$ production since we may misidentify the outgoing gluons as b and $\bar{b}$ jets. Assuming the expected 1% probability of misidentification and applying $60^\circ < \theta < 120^\circ$ jet cut, we estimate $B/S \sim 0.06$.

(ii) There is an admixture of $|J_z| = 2$ production, arising from non-forward going protons [9]. It gives $B/S \sim 0.08$.

(iii) For a massive quark there is a contribution to the $J_z = 0$ LO cross section of order m_b^2/E_T^2, leading to $B/S \sim 0.06$.

At next-to-leading order(NLO), we have the possibility of $gg^{PP} \to b\bar{b}g$ background contributions.

(iv) The extra gluon may go unobserved in the direction of a forward proton. This background may be effectively eliminated by requiring the approximate equality $M_{\text{missing}} = M_{b\bar{b}}$.

(v) The extra gluon is collinear with either the b or $\bar{b}$ jet. We will show that this is suppressed for soft radiation by the specific spin structure of the process[3], and leaves a background coming from three jet $b\bar{b}g$ production with $B/S \sim 0.06$.

We also consider NNLO $b\bar{b}gg$ background contributions.

(vi) There is a NNLO $b\bar{b}$ contribution, which comes from the diagram formed by the product of the NLO amplitudes, which is negligibly small.

[3] This extension of the $J_z = 0$ selection rule suppression to soft radiation is true for soft radiation at any angle

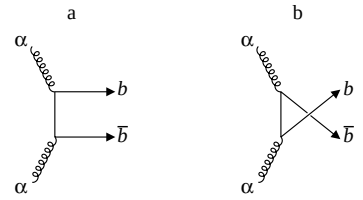

Fig. 2a,b. Colour-singlet $gg \to b\bar{b}$ production, where α denotes the colour of the incoming gluons

(vii) Another source of this background may be called central inelastic production [4], where the $H \to b\bar{b}$ signal or QCD $b\bar{b}$ background is accompanied by central soft gluon radiation. We will show that it causes a 1–2% high mass tail to the 'missing mass' Higgs signal, and again gives a negligible contribution to the background.

Finally, we consider the effects from the collisions of two soft Pomerons. After imposing the missing mass equality, we find that production by Pomeron-Pomeron fusion gives a negligible contribution to both the $H \to b\bar{b}$ signal and the $b\bar{b}$ background. Pomeron-Pomeron fusion is discussed separately in Sect. 2.5.

In summary, taking all these sources of background into account, we would expect a signal/background ratio of about four. The reliability of this signal-to-background estimate, $S/B \simeq 4$, with respect to the theoretical uncertainties, is much better than the factor of two uncertainty in the signal itself. This is because the gap survival probability, S^2, the unintegrated gluon distributions, f_g, the NLO T-factor and even the contribution from the low Q_t non-perturbative domain are common[4] to both the signal, S, and the background, B. Thus the main theoretical uncertainties cancel in the ratio. However, there is another source of uncertainty due to the higher-order virtual corrections to the background processes. We call these, at present unknown, contributions the background K factor. Since we have included the K factor for the Higgs signal in (2), we conservatively take the same K factor for the background. The effect is to reduce S/B to about 3.

Of course, the experimental uncertainties depend on the values of the mass resolutions, $\Delta M_{\text{missing}}$ and $\Delta M_{b\bar{b}}$, the probability to misidentify a gluon as a b-jet, the b-jet tagging efficiency and on the appropriate choice of the jet cone size ΔR; see Sect. 2.6. Here we have taken values which should be attainable, but clearly, in practice, these have to be optimized with reference to the detector, and further gains are possible.

2.4 Determination of the individual backgrounds

Here we quantify each of the potential backgrounds listed above. As a reference point we start with the largest exclusive signal, that is one in which we have no b jet identification. In other words, we have the central production

[4] Except for the $|J_z| = 2$ admixture which has a different structure in the Q_t loop integral for the signal and the background

of a pair of high E_T jets together with tagged outgoing protons. For this situation the ratio of the background to the Higgs signal[5] is

$$\frac{B(gg^{PP}\to gg)}{S(gg^{PP}\to H\to jj)}\simeq 600\left(\frac{\Delta M}{1\,\mathrm{GeV}}\right), \qquad (8)$$

where we have normalised the ratio to the expected experimental missing mass resolution, $\Delta M_{\mathrm{missing}}=1.0\,\mathrm{GeV}$. For clarity, we omit this factor in brackets from now on in this subsection. In (8), the QCD background has been suppressed by imposing the polar angle acceptance cut, $60^\circ<\theta<120^\circ$, in the jet-jet centre-of-mass frame. The cut removes half of the $b\bar{b}$ Higgs signal, but more importantly removes the $gg^{PP}\to gg$ infrared singularity.

Using (8) as a reference point, we now estimate the background/signal for the exclusive process for each of the sources of background listed in Sect. 2.3. We divide them into background contributions at LO, NLO and NNLO.

2.4.1 The LO $b\bar{b}$ backgrounds

(i) Clearly, for the exclusive double-diffractive Higgs signal to be of value, we must reduce B/S of (8). We therefore need to tag both the b and $\bar{b}$ jets. Even so, there is a chance that the gluons are misidentified as b and $\bar{b}$ jets. The expected probability of misidentification is about 1%. Therefore by observing the b and $\bar{b}$ jets we reduce the background by 10^4, and hence

$$\frac{B(gg^{PP}\to gg\to\text{“}b\bar{b}\text{''})}{S(gg^{PP}\to H\to b\bar{b})}\simeq 0.06. \qquad (9)$$

(ii) Of course, there is a background from QCD $b\bar{b}$ production itself. We have emphasized that at LO this vanishes in the massless quark limit, $m_b\to 0$, due to the $J_z=0$ selection rule. However, there is an admixture of $|J_z|=2$ caused by the transverse momenta $\vec{p}_{it}$ of the outgoing protons. In the exact forward direction, the $J_z=0$ selection rule is simply a consequence of angular momentum conservation and the absence of spin-spin correlations between particles separated by a large rapidity gap[6]. However, violation of the rule can come from orbital angular momenta, $p_{it}r$. For our process, the distance r is controlled, not by the size of the proton, but by the effective size of the t-channel gg state. Hence $r\sim 1/Q_t$. Therefore the admixture of $|J_z|=2$ states is strongly suppressed by the ratio $4p_{1t}^2p_{2t}^2/Q_t^4$. It was estimated in [9] that the mean $|J_z|=2$ admixture is less than 1.5%. In addition, $b\bar{b}$ production (even for $|J_z|=2$) is suppressed in comparison to gg production by a factor 27×4 due to the colour and spin $\frac{1}{2}$ character of the quark. The factor represents the exact ratio of the subprocess cross sections at $\theta=90^\circ$ (see (49) and (52) of [4]). Thus we have

$$\frac{B_{|J_z|=2}(gg^{PP}\to b\bar{b})}{S(gg^{PP}\to H\to b\bar{b})} \equiv \frac{\bar{B}}{S}\times(|J_z|=2\ \text{admix.}) \sim \frac{\bar{B}}{S}\times 0.015\sim\frac{600\times 0.015}{27\times 4}\sim 0.08, \qquad (10)$$

where $\bar{B}$ would have been the $gg^{PP}\to b\bar{b}$ background if the $J_z=0$ selection rule had not existed, that is if we had averaged over the incoming gluon helicities in the usual way (as for inclusive production), rather than as in (7).

(iii) A second way to avoid the $J_z=0$ prohibition of the LO background process, $gg^{PP}\to b\bar{b}$, is to allow for the b quark mass. At LO the cross section is suppressed by a factor m_b^2/E_T^2 in comparison to $b\bar{b}$ production $\bar{B}$ in the absence of the $J_z=0$ selection. It is even smaller if we account for the non-Sudakov double-logarithmic suppression [25]. For the acceptance cut $60^\circ<\theta<120^\circ$ the jet transverse energy $E_T\lesssim 10m_b$, and thus

$$\frac{B_{m_b}(gg^{PP}\to b\bar{b})}{S(gg^{PP}\to H\to b\bar{b})}\lesssim\frac{600\times 10^{-2}}{27\times 4}\sim 0.06. \qquad (11)$$

2.4.2 The NLO $b\bar{b}g$ backgrounds

The NLO subprocess $gg^{PP}\to b\bar{b}g$ also generates a background for our exclusive double-diffractive Higgs signal. First recall that the virtual NLO α_S correction has already been included in the $gg\to H$ vertex, (2). Of course, the extra gluon jet may be observed experimentally in the central detector and so these background events can be readily eliminated. The exceptions are the emission of the gluon, first, in one of the beam directions and, second, at large angles, either with small energy $\omega\ll E_T$ or in the b or $\bar{b}$ jet direction.

(iv) Extra gluon radiation in either of the beam directions cannot be observed directly. On the other hand we know it must be energetic. The size of the initial colour-singlet system is $1/Q_0<1\ \mathrm{GeV}^{-1}$. Therefore the transverse momentum of the emitted gluon should be greater than 1 GeV. If the gluon is to go unobserved outside the calorimeter, that is to have $\eta>5$, then the gluon energy $E=p_t\cosh\eta>75$ GeV. This considerably violates the required equality $M_{\mathrm{missing}}=M_{b\bar{b}}$ for a Higgs signal, and so this background can be eliminated.

(v) Now we come to the background associated with large angle gluon emission. First we note that soft gluon emission from the b and $\bar{b}$ quark jets themselves is not a problem, since for this case we retain the cancellation between

[5] Note that the NLO K factor is included for the $gg\to H$ vertex, (2), but in (8) we omit the virtual NLO corrections to the background. For presentation purposes, the denominator in (8) actually refers to only the $H\to b\bar{b}$ component and does not include the $H\to gg$ decays; for $M_H=120$ GeV, including the $H\to gg$ mode would enlarge the denominator by about 10%

[6] Here we refer to the correlation between ‘two spin-flips’. It is very small, and moreover decreases rapidly with beam energy, in soft processes. At small distances it is described by the spin structure function $g_2(x)$, which, in comparison with the unpolarised structure function, is suppressed by a power of x. That is the correlation is suppressed exponentially by the size of the rapidity gap

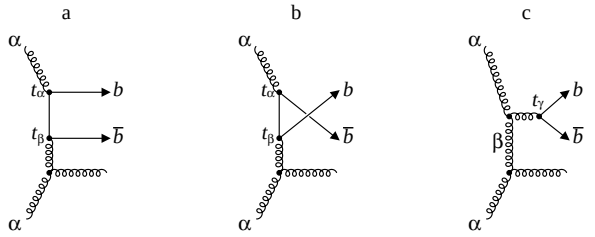

Fig. 3a–c. Colour-singlet $gg \to b\bar{b}g$ production, where α, β and γ are gluon colour labels and where the t_i are the colour matrices for the quark-gluon vertices

the graphs of Fig. 2. Next we note that emission from the virtual b quark line is suppressed by at least a factor of ω/E in the amplitude (and maybe an even higher power[7] of ω/E), where ω and E are, respectively, the energies of a gluon and outgoing b quark in the $gg^{PP} \to b\bar{b}$ centre-of-mass frame. Formally, the factor arises from the large virtuality of the extra b quark propagator, and reflects the fact that the $1/\omega$ formation time of the extra soft gluon is much larger than the lifetime of the virtual t channel b quark.

The potential danger is emission from one of the incoming t channel gluons. At first sight it appears to be a rather large contribution of order $(\alpha_S N_C/\pi)\ln(M_H/Q_0)$, where the large log comes from the $d\omega/\omega$ integration embracing soft gluon emission. On the other hand, to accuracy ω/E, we deal with pure classical emission which does not change the spin structure of the amplitude. Therefore we might expect the same cancellation between the graphs of Fig. 3a and b as was obtained in Fig. 2. But now the $b\bar{b}$ system is in a *colour octet* state and the commutator

$$[t_\alpha, t_\beta] = i f_{\alpha\beta\gamma} t_\gamma \tag{12}$$

spoils the cancellation. Here t_i are the colour matrices of the quark-gluon vertices. All is not lost, however, since now we have a third diagram, Fig. 3c, which has precisely the colour and spin structure to restore the cancellation. Thus soft gluon emissions from the initial colour-singlet gg^{PP} state factorize (see, for example, [28]) and, due to the overriding $J_z = 0$ selection rule, QCD $b\bar{b}$ production is still suppressed. In this way the $\ln(M_H/Q_0)$ contribution is neutralised and we are left with $O(\alpha_S)$ large angle hard gluon emission. Such three jet $b\bar{b}g$ production can be observed and excluded experimentally, except for hard gluon radiation along the b and $\bar{b}$ jet directions. If we denote the cone angle needed to separate the g jet from the b (or $\bar{b}$) jet by ΔR, then the expected background from unresolved three jet events is of about[8]

$$\begin{aligned}(\alpha_S C_F/2\pi)\,(\Delta R)^2 \bar{B}(gg^{PP} \to b\bar{b}) \\ \sim\ 0.01\bar{B}(gg^{PP} \to b\bar{b})\end{aligned} \tag{13}$$

for $\Delta R \sim 0.5$, where $C_F = (N_C^2 - 1)/2N_C = 4/3$. In (13) we sum the contributions from gluon emission in the directions of both b and $\bar{b}$ jets. Recall that $\bar{B}$ is the $gg^{PP} \to b\bar{b}$ rate in the absence of the $J_z = 0$ selection rule. Noting (8) and (10), we thus see that we have a background-to-signal ratio of

$$\frac{B(gg^{PP} \to b\bar{b}g)}{S(gg^{PP} \to H \to b\bar{b})} \sim \frac{0.01 \times 600}{27 \times 4} \sim 0.06. \tag{14}$$

This source of background may be further suppressed by choosing smaller size b and $\bar{b}$ jet cones, ΔR. The price is the presence of an extra Sudakov form factor which accounts for the absence of bremsstrahlung outside the more confined cone, that is radiation which would normally be allowed in the jet hadronisation. As we need to exclude only hard gluon radiation, this is a single, not double, logarithmic form factor. It is present in both the signal and the background, and so does not change the S/B ratio. However, it reduces the number of selected events. The form factor is estimated to be $\sim \Delta R^{0.8}$. On the other hand it is possible that if we take a smaller ΔR then we will improve the efficiency of the b and $\bar{b}$ identification. In this way, the Sudakov suppression arising from a smaller ΔR could be partly compensated. Of course, in practice, we should choose the jet cone size ΔR to optimize the significance of the signal.

2.4.3 The NNLO $b\bar{b}gg$ background

(vi) There is a contribution to the $b\bar{b}$ QCD background cross section at NNLO, which comes from the 'square' of NLO amplitudes, in which the $J_z = 0$ amplitude for the $gg^{PP} \to b\bar{b}$ subprocess does not vanish, even in the massless quark limit. Note that, for the imaginary part of the one-loop box diagram, the arguments based on T invariance are redundant [24]. However, numerically, this $b\bar{b}$ background contribution appears to be very small (see [30] for an explicit calculation in the case of $\gamma\gamma(J_z = 0) \to q\bar{q}$, and also [25]). This is because it is suppressed by the two-loop factor $(N_C\alpha_S/4\pi)^2$, where α_S is taken at a large scale of the order of $M_H/2$. Therefore the corresponding ratio B/S does not exceed 0.01, and can be safely neglected.

(vii) Finally, there is a background to $pp \to p + (H \to b\bar{b}) + p$ due to central inelastic production, where the $b\bar{b}$ pair (or Higgs boson) is accompanied by soft QCD radiation in the central region, see Fig. 4a. Hard radiation is excluded by requiring the mass equality $M_{\text{missing}} = M_{b\bar{b}}$, as noted above. Moreover, recall that soft radiation from the final b or $\bar{b}$ quark lines is already included in the jet finding algorithm. So we are left with central soft radiation from the t channel lines. Due to factorization of soft gluon radiation from the colour-singlet gg^{PP} state (see, for example, [28]), this emission does not alter the signal-to-background ratio. However, it could blur out the sharp missing-mass peak of the Higgs signal. Fortunately, the phase space for such radiation is strongly limited by requiring the $M_{\text{missing}} = M_{b\bar{b}}$ mass balance. Consider the

[7] An explicit calculation for the $\gamma\gamma(J_z = 0) \to b\bar{b}g$ cross section shows a $(\omega/E)^4$ suppression, see for example [24]. This is a consequence of the Low-Burnett-Kroll theorem [26], see [27]

[8] We thank Andrei Shuvaev for calculating this higher-order contribution (see also [29], where the formalism to obtain the helicity amplitudes for the $gg \to b\bar{b}g$ subprocess is given)

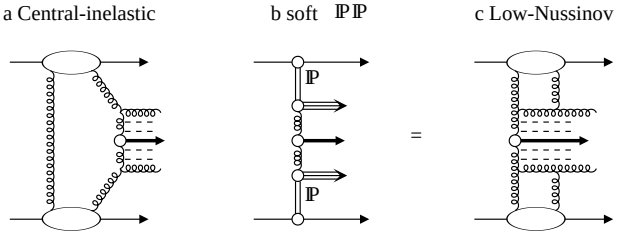

Fig. 4a–c. Double-diffractive production of a Higgs boson (shown by the *bold* central arrow) accompanied by gluon emission in diagram **a** and by Pomeron remnants in diagram **b**. Diagram **c** shows the Pomeron-Pomeron production process from a QCD viewpoint, in which each Pomeron is represented by two-gluon exchange

emission of two extra soft gluons, that is the NNLO subprocess $gg^{PP} \to Hgg$. (One extra gluon cannot be produced together with the Higgs boson from the colour-singlet gg^{PP} state, and the $b\bar{b}g$ QCD background has already been considered in (iv) above.) Using factorization, the probability of the emission of the extra two gluons is

$$\left(\frac{1}{N_C^2-1}\right)\frac{1}{2!}\left[2\left(\frac{\alpha_S N_C}{\pi}\right)\int\frac{d\omega}{\omega}\frac{dp_t^2}{p_t^2}\right]^2, \qquad (15)$$

where the first factor reflects colour-singlet production, $1/2!$ accounts for the identity of the two gluons, the factor 2^2 allows for emission from both incoming gluons and the familiar double-log accounts for emission with gluon energies $\omega > p_t > Q_0$, as discussed before. The energy ω may be bounded by experimentally requiring $M_{\rm missing} = M_{b\bar{b}}$. If we assume an experimental resolution $\Delta M_{b\bar{b}} = 10$ GeV and take $\alpha_S = 0.25$ at the low Q_0 scale, then the probability (15) is about 1–2%. This Hgg background does not affect the significance of the exclusive Higgs signal, but produces a small tail on the high side of the missing mass peak. Due to the factorization of soft gluon emission, which we discussed in (v), the direct QCD $b\bar{b}gg$ production is additionally suppressed by the $J_z = 0$ selection rule, and is hence negligible.

2.5 Production by soft pomeron-pomeron collisions

In addition to the central inelastic production, Fig. 4a, studied above, there exists another class of diagrams, Figs. 4b or c, in which the colour flow is screened in a different way. These diagrams describe production by soft Pomeron-Pomeron inelastic collisions[9]. Within this approach, one may use the factorizable, a la Ingelman-Schlein [31], model in which the Higgs (or $b\bar{b}$ pair) is created by a $gg \to H$ (or $gg \to b\bar{b}$) subprocess that is driven by the 'gluon structure functions' of the Pomerons themselves [32–34].

Here we check the size of the background to the exclusive Higgs signal which comes from soft Pomeron-Pomeron collisions. We use the Donnachie-Landshoff parameterization [35] to calculate the Pomeron flux and take the gluon structure function of the Pomeron to be $zg^P(z) \le 0.7$, which is consistent with the H1 analysis [36]. Besides the relatively low values of the Pomeron flux and of g^P, the main suppression comes from the requirement that the Pomeron-Pomeron mass ($M_{PP} = M_{\rm missing}$) measured by the tagged protons, should lie within the $M_{b\bar{b}} + \Delta M_{b\bar{b}}$ mass interval. This mass balance requires that the gluon in the Pomeron has momentum fraction z close to 1, where the structure function $g^P(z)$ becomes small. To allow for uncertainties in the H1 analysis we conservatively take $g^P(z) = 0.7$, even in this large z domain. Then the cross section for the Pomeron-Pomeron fusion subprocess is, see [4]

$$\sigma(\mathbb{PP} \to b\bar{b}) = \int dz_1 g^P(z_1) \int dz_2 g^P(z_2)\hat{\sigma}(gg \to b\bar{b}) \lesssim (0.7)^2\, 2\left(\frac{\Delta M_{b\bar{b}}}{M_{PP}}\right)^2 \hat{\sigma}(gg \to b\bar{b}). \qquad (16)$$

We mentioned that the phenomenological flux of the soft Pomeron is relatively small. Indeed, for $M_{PP} = 120$ GeV the effective Pomeron-Pomeron luminosity is a factor two smaller than the corresponding luminosity for the exclusive process, which was calculated in terms of the unintegrated gluon distributions (compare the curves denoted by 'soft $\mathbb{PP}$' and 'excl' in Fig. 2c of [4]). So, finally, the suppression factor in going from the exclusive process to Fig. 4b is

$$\frac{1}{2}\left(\frac{\Delta M_{b\bar{b}}}{M_{PP}}\right)^2 \lesssim 4\times 10^{-3}, \qquad (17)$$

if we take $\Delta M_{b\bar{b}} = 10$ GeV. Even though the $J_z = 0$ selection rule is absent for Pomeron-Pomeron production, it gives a background which is much less than the background caused by the $|J_z| = 2$ admixture of (ii).

If we consider Pomeron-Pomeron production of the $H \to b\bar{b}$ signal, then there is an additional suppression coming from a factor $1/\left(2(N_C^2-1)\right)$, since the gluons producing the Higgs must have the same helicity and colour. In practice such a soft Pomeron-Pomeron source of the signal appears to be very small, even for $M_{PP} \gg M_H$.

Our estimates of the inclusive double-diffractive background $b\bar{b}$ production, when translated to Tevatron energies, agree reasonably well with the Monte Carlo simulation of [32]. Of course, in [32] only the contribution of Fig. 4b was considered, but the result was normalized to the CDF data [37] and in this way the major contribution coming from Fig. 4a type of diagrams was accounted for. On the other hand, we do not reproduce the results of [33].

2.6 Experimental issues concerning $pp \to p + H + p$

The most prominent characteristic feature of diffractive Higgs production is the formation of rapidity gaps between

[9] From a QCD viewpoint the soft Pomeron-Pomeron interaction, Fig. 4b, should be regarded as Fig. 4c where the soft Pomerons are replaced by (Low-Nussinov) two-gluon exchange. We note that diagram 4(c) contains an extra factor of α_S, as compared to diagram 4(a). Of course the coupling is taken at a low scale, but nevertheless we should not be surprised when we find the contribution of 4(c) is less than that of 4(a)

the Higgs decay products and the scattered protons. The gaps will be however of limited use at the LHC collider, when the machine is operated at medium ($10^{33}\,\mathrm{cm}^{-2}\mathrm{s}^{-1}$) and high ($10^{34}\,\mathrm{cm}^{-2}\mathrm{s}^{-1}$) luminosity, due to pile-up, as discussed in Sect. 3.2. To select these events in the experiment it is important to tag the scattered protons. This has furthermore the crucial advantage that the mass of the Higgs particle can be precisely reconstructed from the missing mass to the protons, as detailed below. Due to the relatively low mass of the central (Higgs) system, the scattered protons have small ξ values, in the range of 10^{-3}–10^{-2}, where ξ is the momentum fraction lost by the proton in the interaction. A classical technique to detect scattered protons at small t and with small relative momentum loss, is by using so-called Roman Pot detectors. Recently a new type of detectors, called microstations [38], has been proposed for this purpose. Studies of the LHC beam optics [39] reveal that, in order to access these small ξ values, the Roman Pot detectors or microstations need to be installed at about 425 m from the interaction region. These detectors can have an acceptance in ξ down to 1–2$\times 10^{-3}$, and a parametrization of the acceptance was included in the event estimates in this paper.

In order to efficiently record and measure the diffractively scattered protons in Roman Pot detectors or microstations, they have to be sufficiently separated from the beam particles. The detectors, which are located at 420 m and 430 m from the interaction point, could then be used to define the proton momenta by measuring, with respect to the beam axis, the difference in horizontal displacement at the two locations as a function of the average proton deflection.

We observe that a variation of $\Delta\xi = 5 \times 10^{-4}$ produces a 80 μm difference in the horizontal displacement of a diffractively scattered proton. With state-of-the-art silicon microstrip detectors this difference can be measured with a precision of the order of 5μm. The expected momentum spread of the beam protons is $\Delta\xi/\xi = 10^{-4}$. For a symmetric event configuration ($\Delta = |\xi_1 - \xi_2| \leq 0.04$), we then expect in the most optimistic case a mass resolution of the order of $\Delta M_{\mathrm{missing}}/M_{\mathrm{missing}}$ better than 1% [39]. This leads to the value $\Delta M_{\mathrm{missing}} = 1$ GeV, which is used in Table 1.

The acceptance of diffractively scattered protons is limited by the minimum measurable deflection and, on the other hand, by the aperture of the last dipole magnet (B11) of the LHC lattice, i.e., 30mm, and leads to a range of observable missing masses of 20 GeV $< M_{\mathrm{missing}} <$ 160 GeV. A similar reason restricts the observable rapidity interval of the central produced (Higgs) system. Since we do not measure ξ smaller than 1–2$\times 10^{-3}$, we are unable to select events with Higgs rapidity $|y_H|$ >1.2–1.6. As a result, the efficiency of proton tagging is 60% for $M_H = 120$ GeV. In calculating acceptances, the detector edge effects (guard ring, shielding, possible insulation layer, etc.) play a significant role and can be further minimised. Effects due to detector alignment accuracy have still to be assessed carefully.

For selecting the central diffractive events, a sufficient suppression of the huge non-diffractive event rates has to be provided. An event selection strategy could consist of the following three steps:

(i) At the first trigger level, select events with a pair of jets in the central detector ($|\eta| < 2.5$) each with $E_T >$ 40 GeV and with the difference between their azimuthal angles $\phi_1 - \phi_2 = 180^\circ$ (within a given cell size of $\Delta\eta \times \Delta\phi$). Furthermore, one can make use of the absence of significant additional central activity in these events.
(ii) At a later stage of data collection, or in off-line analysis, use the forward-backward proton measurement to calculate the missing mass, and
(iii) analyse the events of interest by using the central detector data.

With condition (i), a relative suppression of background to central diffractive events of the order of 10^4 is obtained. Therefore, a well recordable first level trigger rate may be achieved [39].

Pile-up events will also be important for the Roman Pot detectors. The PYTHIA [19] Monte Carlo program was used to estimate the probability to have an additional proton accepted on one side of the interaction region from single soft diffraction for the different luminosities, and amounts to 8% (medium luminosity), 40% (high luminosity) and 200% (SLHC[10]). Hence at the SLHC special care is needed to control the combinatorics generated by background from pile-up events. Since by then the mass of the Higgs to some accuracy will be known, an appropriate mass window can be chosen to select genuine scattered protons that belong to the diffractive Higgs event.

The next issue is the efficiency ε_b of tagging a b jet. The value is correlated with the probability $P(g/b)$ to misidentify a gluon as a b jet. As we have seen in (i) of Sect. 2.4.1, we require $P(g/b) = 0.01$ to reduce the gg background to an acceptable level. For this value of $P(g/b)$, the present estimate of the efficiency of b and $\bar{b}$ tagging is $(\varepsilon_b)^2 = 0.3$, but it is not inconceivable that this could be improved to a larger value, perhaps as large as $(\varepsilon_b)^2 = 0.6$. If it turns out that this is impossible for $P(g/b) = 0.01$, then it is better to accept a worse misidentification probability $P(g/b)$ in order to obtain a higher value of $(\varepsilon_b)^2$. This will raise the background, but will result only in a relatively small reduction in the significance of the signal. For this reason we use $(\varepsilon_b)^2 = 0.6$ in our estimates.

Therefore the event rate in (c) of Table 1 includes a factor 0.6 for the efficiency associated with proton tagging and 0.6 for b and $\bar{b}$ tagging. Besides this the signal has been multiplied by 0.5 for the jet polar angle cut and 0.67 for the $H \to b\bar{b}$ branching fraction. Hence the original ($\sigma = 3$ fb) $\times$ ($\mathcal{L} = 30\,\mathrm{fb}^{-1}$) = 90 events is reduced to an observable signal of 11 events, as shown in Table 1.

[10] The Super LHC luminosity is taken to be $10^{35}\,\mathrm{cm}^{-2}\mathrm{s}^{-1}$

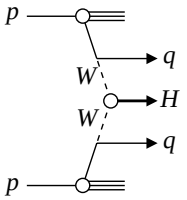

Fig. 5. Higgs production by weak boson fusion at the LHC, which is accompanied by forward and backward going quark jets

3 Higgs production by Weak Boson Fusion (WBF)

We have seen in Sect. 2 that the selection of events with large rapidity gaps is an effective way of suppressing the QCD background. Recall that rapidity gaps appear naturally in Weak Boson Fusion (WBF) [11,13]. One can thus exploit this property to suppress the QCD background and to observe a light Higgs boson produced by WBF via its main $H \to b\bar{b}$ decay mode, in addition to the rather rare decay modes, $\tau\tau$, WW^*, etc. usually proposed for WBF, see Table 1 and [2,5,40]. Another special feature of Higgs production by WBF is the high momentum transfer, $p_t \sim O(M_W)$. The hard subprocess may be written as

$$qq \to \text{jet}\, W\, W\, \text{jet} \to \text{jet} + H + \text{jet} \qquad (18)$$

where again a + sign denotes a rapidity gap. The process is sketched in Fig. 5.

3.1 The WBF $H \to b\bar{b}$ signature

Two alternative signatures of the WBF $H \to b\bar{b}$ events exist. First, we may select events with large p_t (quark) jets in the forward and backward directions, separated from the $H \to b\bar{b}$ decay by rapidity gaps. Alternatively we may select events with a high q_t Higgs (or $b\bar{b}$ system), with rapidity gaps on either side.

In practice the $H \to b\bar{b}$ decay should be observed in the central detector. We choose the rapidity $|y_{\text{Higgs}}| < 2.1$, and impose the polar angular cut $60^\circ < \theta < 120^\circ$ on the b and $\bar{b}$ jets (as discussed in Sect. 2.4). The accompanying quark jets are observed in the forward and backward calorimeters. For these we take[11] $3 < |\eta_{\text{jet}}| < 5$. The results presented in the upper entry of (f) in Table 1 correspond to the selection of events with $p_t > 30$ GeV (quark) jets in the forward and backward directions, which are separated from $H \to b\bar{b}$ by rapidity gaps. For the alternative signature, shown by the lower entry of (f) in Table 1, we impose the cut $q_t > 30$ GeV on the $H \to b\bar{b}$ system. The detailed kinematics are described in [41].

The leading order QCD background for process (18), with $H \to b\bar{b}$, is rather large, even after imposing the presence of rapidity gaps and the high p_t (or q_t) cuts. There is, therefore, no need for a detailed discussion of the higher-order background contributions in this case. Although S/B is relatively small, the cross section is considerably larger than for the exclusive process and so the significance of the signal looks good. In fact in some respects, this signal is similar to the search for the decay $H \to \gamma\gamma$ in an inclusive process; compare entries (a) and (f) of Table 1.

The main problem is that it is hard to identify rapidity gaps in inclusive reactions at high luminosity, where pile-up becomes significant. The possibility to identify the vertex of Higgs production, and to separate off the particles associated with other interactions, is discussed in Sect. 3.2.

The survival probability S^2 of the rapidity gaps to soft rescattering is an ingredient in the calculation of both the signal and the background of these $j + (b\bar{b}) + j$ events. It is informative to discuss the values of S^2 that are obtained. Recall that the survival of the gaps, at the hadronic level, are computed using a two-channel eikonal model for soft rescattering [17,23]. For WBF the probability S^2 depends more sensitively on the model than the previous calculation of S^2 for $pp \to p + (b\bar{b}) + p$ of Sect. 2. The incoming partons which participate in the WBF subprocess $qq \to q + (b\bar{b}) + q$ are rather hard. They have large x and a larger scale. Thus in a multi-channel eikonal approach, it is probable that such partons belong to the component with the lower absorptive cross section. Hence the survival probability S^2 is larger. Clearly the results will depend on how the partons (of the global analysis[12]) are distributed between the different diffractive eigenstates, that is different channels of the eikonal.

Here we have used model II of [23], which looks the most realistic and which provides a good description of the CDF data for the diffractive production of a pair of high E_T jets. For the first WBF signature (upper entry of (f) in Table 1), the corresponding values of S^2 are 0.30 and 0.25 for the signal and background respectively; whereas for the Higgs $q_t > 30$ GeV signature (lower entry) the values of S^2 are 0.26 and 0.21 for the signal and background respectively.

In model I of [23], which may be regarded as an extreme case, it is assumed that all the valence quarks are concentrated in the eikonal component with the smaller absorption cross section and the gluons in that with the larger cross section[13]. In this case the QCD $b\bar{b}$ background, which originates mainly from gluons, has gaps with a smaller survival probability ($S^2 = 0.09$ for both signatures (f) of Table 1) and the significance of WBF Higgs signal would be increased to about 8σ.

3.2 Experimental issues associated with Higgs production by WBF with rapidity gaps

Both the ATLAS and CMS experiments at the LHC prepare to measure jets and energy flows as far out as $\eta = 5$,

[11] If we were to enlarge the coverage up to $\eta_{\text{jet}} = 7$ then we would increase the cross section by only 3%, leaving the signal-to-background ratio essentially unaltered

[12] We use MRST partons [42]

[13] This was the model used to generate the results in the lower half of Table 1 of [41]

matching the cuts in Sect. 3.1. Hence the forward jets can be tagged and measured. For the trigger typically four jet final states need to be selected, supplemented with topological requirements, if one wants to go down in jet E_T threshold as much as 30 GeV.

When the LHC collider operates at medium and high luminosity, the recorded events will be plagued by overlap interactions in the same bunch crossing. At medium luminosity (i.e., 10^{33} cm^{-2}s^{-1}) on average 2.3 inelastic events are expected to be produced in each bunch crossing. Hence the rapidity gaps will often be destroyed by these additional pile-up events. In particular, for the high luminosity operation (10^{34} cm^{-2}s^{-1}), on average 22 additional events are overlaid on top of the signal event, which will essentially always destroy the gap.

It is, however, possible to use the detector information to try to reconstruct the gap in the hard scattering events. The vertices of the individual collisions will be (non-uniformly) distributed along the beam axis in the interaction region over a distance of 10–20 cm. The precise tracking subdetectors of the experiments will, however, allow the reconstruction of vertex positions with a precision of a few tens of microns, and even soft tracks can be associated to their corresponding vertex with a precision of a fraction of a millimeter. Thus one can imagine an event selection that checks for rapidity gaps based on the charged particles associated with the proper vertex. Furthermore, the transverse energy of particles from the soft overlap events is generally low and, for example, considering only particles with an E_T value larger than of order 1–2 GeV will often reveal the underlying rapidity gap of the hard scattering event.

All rapidity gaps in the events should be detectable by vertex and/or soft energy cuts particularly for the data taken at medium luminosity, and probably also for high luminosity data samples. However, it is unlikely that these techniques can be used for the SLHC type of luminosity of 10^{35} cm^{-2}s^{-1}.

4 Discussion

4.1 Measurement of Higgs couplings

As emphasized in the Introduction there is no single obvious best discovery channel for a light Higgs boson at the LHC. Rather the search should employ all possibilities. The comparability of channels has some advantages in the measurement of Higgs couplings. The Double-diffractive Higgs production processes (entries (c) and (d) of Table 1) are mediated by the subprocess $gg \to t\bar{t} \to H$, and are thus proportional to the H–$t\bar{t}$ coupling (squared). The same is true for production processes (a) and (b). For process (a) the $H \to \gamma\gamma$ decay is mainly controlled by the H–WW coupling, while processes (b) and (c) are proportional to the H–$b\bar{b}$ coupling (squared). From Table 1 we note the relatively large significance of the WBF processes, (e) and (f), in which the Higgs signal is separated from forward and backward high p_t jets by rapidity gaps. These WBF processes are, of course, driven by the H–WW coupling. If the $H \to \tau\tau$ decay process is observed, then we can study the Higgs-lepton coupling. The estimates presented in Table 1 for this $qq \to qHq \to j\tau\tau j$ process are taken from [2]. The values agree reasonably well with the results[14] shown in Table 1 of [41]. Thus by measuring combinations of the above processes it is possible to determine the Higgs coupling to b and t quarks, W bosons and the τ lepton.

4.2 Conclusion

This paper has concentrated on the production of a light Higgs boson accompanied by rapidity gaps. In Sect. 2 we discussed exclusive double-diffractive (CP-even) Higgs production

$$pp \to p + H(b\bar{b}) + p, \tag{19}$$

and in Sect. 3, Weak Boson Fusion via the subprocess

$$qq \to q + H + q \to \text{jet} + b\bar{b} + \text{jet}. \tag{20}$$

In both cases we estimated the cross section for the $H \to b\bar{b}$ signal and for the QCD $b\bar{b}$ background, at the LHC. The results obtained are summarised in entries (c) and (f) of Table 1.

Provided that appropriate proton taggers are installed (see Sect. 2.6), process (19) has the special advantage that the Higgs can be identified by a sharp peak in the protons' 'missing mass' spectrum and, simultaneously, as a peak in the $b\bar{b}$ mass spectrum. The required equality $M_{\text{missing}} = M_{b\bar{b}}$, allowing for resolution, is of great value, not only to establish the signal, but also to suppress the $b\bar{b}+ng$ background. In addition, the existence of a $J_z = 0$ selection rule automatically greatly suppresses the leading order (LO) QCD $b\bar{b}$ background. We estimated the LO, NLO and NNLO contributions to the $b\bar{b}+ng$ background. It turned out that, for production from a colour-singlet two-gluon system, the special colour and helicity structure of the subprocess is such that even the higher order (NLO,...) contributions to the background are suppressed. In summary, we find[15]

$$\frac{\text{Signal}}{\text{Background}} \simeq 3 \tag{21}$$

for the exclusive double-diffractive production of a light Higgs boson, decaying via $b\bar{b}$, at the LHC. The favourable signal-to-background ratio is offset by a low event rate, caused by the necessity to preserve the rapidity gaps so as to ensure an exclusive signal. Nevertheless, entry (c) of Table 1 shows that the signal has comparable signifi-

[14] The $\tau\tau$ results in Table 1 of [41] included a 10% efficiency to identify the two τ leptons

[15] Here, and in Table 1, we (conservatively) assume that the higher-order virtual contribution to the background has approximately the same relative size (that is the same K factor) as the signal

cance[16] to the standard $H \to \gamma\gamma$ and $t\bar{t}H$ search modes (entries (a) and (b)).

The cross section for the production of a 120 GeV Higgs boson at the LHC, via the exclusive $pp \to p+H+p$ process, was calculated to be 3 fb (see Sect. 2.1), but after including the $H \to b\bar{b}$ branching fraction, and the acceptance and efficiency cuts, we arrive at only 12% of the signal. The breakdown of the depletion of the signal is summarized at the end of Sect. 2.6. Thus for an integrated luminosity of 30 fb^{-1} (300 fb^{-1}) we would register 11 (110) events. Noting the B/S ratio of (21), we see that these signals have a significance of about 3σ and 9σ respectively. We estimate a factor of two uncertainty in the cross section for this exclusive Higgs signal (see Sect. 2.2), but a much better reliability for the signal-to-background prediction, (21), since the main theoretical uncertainties cancel in the ratio (see Sect. 2.3).

The Weak Boson Fusion signal, (20), does not need the installation of proton taggers, and has a favourable significance; see Sect. 3 and Table 1. As discussed in Sect. 3.2, the main problem is to identify these rapidity gap events from the additional pile-up events, that is from overlap interactions in the same bunch crossing. There is good reason to believe that, at the medium luminosity of 10^{33}cm^{-2} s^{-1} of the LHC, the problem can be overcome, and that we can go a considerable way to achieving the numbers quoted in entry (f) of Table 1.

In conclusion, we have shown how the rapidity gap processes, (19) and (20), may play a key role in identifying and studying a light Higgs boson at the LHC.

Acknowledgements. We thank Andrei Shuvaev for valuable help in the calculations of the QCD $b\bar{b}$ background, and Marco Battaglia, Michael Kraemer, Jerry Lamsa, James Stirling, Theodore Todorov and Peter Williams for useful discussions. One of us (VAK) thanks the Leverhulme Trust for a Fellowship. This work was partially supported by the UK Particle Physics and Astronomy Research Council, by the Russian Fund for Fundamental Research (grants 01-02-17095 and 00-15-96610) and by the EU Framework TMR programme, contract FMRX-CT98-0194 (DG 12-MIHT).

References

1. D. Cavalli et al., hep-ph/0203056
2. D. Zeppenfeld, R. Kinnunen, A. Nikitenko, E. Richter-Was, Phys. Rev. D **62**, 013009 (2000)
3. V. Drollinger, T. Müller, D. Denegri, CMS note, hep-ph/0111312; J. Goldstein, C.S. Hill, J. Incandela, S. Parke, D. Rainwater, D. Stuart, Phys. Rev. Lett. **86**, 1694 (2001)
4. V.A. Khoze, A.D. Martin, M.G. Ryskin, Eur. Phys. J. C **23**, 311 (2002)
5. D. Zeppenfeld, hep-ph/0203123; N.Kauer, T. Plehn, D. Rainwater, D. Zeppenfeld, Phys. Lett. B **503**, 113 (2001)
6. V. Drollinger, T. Müller, D. Denegri, CMS note, hep-ph/0201249
7. Z. Bern, L. Dixon, C. Schmidt, hep-ph/0206194
8. V.A. Khoze, A.D. Martin, M.G. Ryskin, hep-ph/0006005, in Proc. of 8th Int. Workshop on Deep Inelastic Scattering and QCD (DIS2000), Liverpool, eds. J. Gracey, T. Greenshaw (World Scientific, 2001), p.592
9. V.A. Khoze, A.D. Martin, M.G. Ryskin, Eur. Phys. J. C **19**, 477 (2001), erratum C **20**, 599 (2001)
10. V.A. Khoze, A.D. Martin, M.G. Ryskin, Eur. Phys. J. C **14**, 525 (2000)
11. Yu.L. Dokshitzer, S.I. Troian, V.A. Khoze, Sov. J. Nucl. Phys. **46**, 712 (1987)
12. Yu.L. Dokshitzer, V.A. Khoze, T. Sjöstrand, Phys. Lett. B **274**, 116 (1992)
13. J.D. Bjorken, Int. J. Mod. Phys. A **7**, 4189 (1992), Phys. Rev. D **47**, 101 (1993)
14. R.S. Fletcher, T. Stelzer, Phys. Rev. D **48**, 5162 (1993)
15. A.D. Martin, M.G. Ryskin, Phys. Rev. D **57**, 6692 (1998)
16. A.G. Shuvaev, K.J. Golec-Biernat, A.D. Martin, M.G. Ryskin, Phys. Rev. D **60**, 014015 (1999)
17. V.A. Khoze, A.D. Martin, M.G. Ryskin, Eur. Phys. J. C **18**, 167 (2000)
18. A. Edin et al., Phys. Lett. B **366**, 371 (1996), A. Edin et al., Z. Phys. C **75**, 57 (1997)
19. T. Sjöstrand et al., Comput. Phys. Commun. **135**, 238 (2001), T. Sjöstrand, Comput. Phys. Commun. **82**, 74 (1994)
20. R. Enberg et al., Phys. Rev. D **64**, 114015 (2001)
21. R. Enberg, G. Ingelman, A. Kissavos, N. Timneanu, hep-ph/0203267
22. CDF collaboration, T. Affolder et al., Phys. Rev. Lett. **84**, 5043 (2000)
23. A.B. Kaidalov, V.A. Khoze, A.D. Martin, M.G. Ryskin, Eur. Phys. J. C **21**, 521 (2001)
24. D.L. Borden, V.A. Khoze, W.J. Stirling, J. Ohnemus, Phys. Rev. D **50**, 4499 (1994)
25. V.S. Fadin, V.A. Khoze, A.D. Martin, Phys. Rev. D **56**, 484 (1997), M. Melles, W.J. Stirling, V.A. Khoze, Phys. Rev. D **61**, 054015 (2000)
26. F.E. Low, Phys. Rev. **110**, 974; (1958) T.H. Burnett, N.M. Kroll, Phys. Rev. Lett. **20**, 86 (1968)
27. Yu.L. Dokshitzer, V.A. Khoze, W.J. Stirling, Nucl. Phys. B **428**, 3 (1994)
28. B.I. Ermolaev, V.S. Fadin, L.N. Lipatov, Sov. J. Nucl. Phys. 45 (1987) 508
29. L. Dixon, TASI lectures, 1995, hep-ph/9601359
30. G. Jikia, A. Tkabladze, Phys. Rev. D **54**, 2030 (1996)
31. G. Ingelman, P.E. Schlein, Phys. Lett. B **152**, 256 (1985)
32. B.E. Cox, J.R. Forshaw, B. Heinemann, hep-ph/0110173
33. M. Boonekamp, R. Peschanski, C. Royon, Phys. Rev. Lett. **87**, 251806 (2001)
34. M. Boonekamp, A. De Roeck, R. Peschanski, C. Royon, hep-ph/0205332
35. A. Donnachie, P.V. Landshoff, Phys. Lettt. B **296**, 227 (1992)
36. H1 collaboration: C. Adloff et al., Z. Phys. C **76**, 613 (1997)
37. CDF Collaboration, T. Affolder et al., Phys. Rev. Lett., **85**, 4215 (2000)
38. V.P. Nomokonov for the Helsinki Group in Forward Physics, Luminosity Determination at LHC, Helsinki, Finland, 31 October to 4 November 2000, World Scientific (2001) 164, ed. R. Orava, K. Huitu, V. Khoze, S. Tapprogge

[16] However, when the NLO contributions to the $H \to \gamma\gamma$ signal and background are included, the significance of this signal is increased to about 7σ for 30 fb^{-1} LHC luminosity and Higgs mass $M_H \simeq 120$ GeV [7]

39. R. Orava, Diffraction at LHC, Workshop on Diffractive Physics, LISHEP 2002, Rio de Janeiro, Brasil, 4–8 February 2002, acceptance, resolution figures refer to the simulation studies by J. Lamsa (Iowa Sate University, Ames, Ill.) and R. Orava
40. D. Rainwater, D. Zeppenfeld, K. Hagiwara, Phys. Rev. D **59**, 014137 (1999), D. Zeppenfeld, D. Rainwater, Phys. Rev. D **60**, 113004 (1999)
41. V.A. Khoze, A.D. Martin, M.G. Ryskin, Eur. Phys. J. C **21**, 99 (2001)
42. A.D. Martin, R.G. Roberts, W.J. Stirling, R.S. Thorne, Eur. Phys. J. C **4**, 463 (1998)